The Astrophysical Journal, 834:113 (11pp), 2017 January 10 doi:10.3847/1538-4357/834/2/113

RADIO-WEAK BL LAC OBJECTS IN THE *FERMI* ERA

F. Massaro[1,2,3], E. J. Marchesini[1,4,5], R. D'Abrusco[6], N. Masetti[7,8], I. Andruchow[4,5], and Howard A. Smith[6]
[1] Dipartimento di Fisica, Università degli Studi di Torino (UniTO), via Pietro Giuria 1, I-10125 Torino, Italy
[2] Istituto Nazionale di Fisica Nucleare, Sezione di Torino, via Pietro Giuria 1, I-10125 Torino, Italy
[3] INAF—Osservatorio Astrofisico di Torino, via Osservatorio 20, I-10025, Pino Torinese, Italy
[4] Facultad de Ciencias Astronómicas y Geofísicas, Universidad Nacional de La Plata, Paseo del Bosque, B1900FWA, La Plata, Argentina
[5] Instituto de Astrofísica de La Plata, CONICET–UNLP, CCT La Plata, Paseo del Bosque, B1900FWA, La Plata, Argentina
[6] Smithsonian Astrophysical Observatory, 60 Garden Street, 02138 Cambridge (MA), USA
[7] INAF—Istituto di Astrofisica Spaziale e Fisica Cosmica di Bologna, via Gobetti 101, I-40129, Bologna, Italia
[8] Departamento de Ciencias Físicas, Universidad Andrès Bello, Fernàndez Concha 700, Las Condes, Santiago, Chile
Received 2016 July 11; revised 2016 September 18; accepted 2016 September 19; published 2017 January 6

ABSTRACT

The existence of "radio-weak BL Lac objects" (RWBLs) has been an open question, and has remained unsolved since the discovery that quasars could be radio-quiet or radio-loud. Recently, several groups identified RWBL candidates, mostly found while searching for low-energy counterparts of the unidentified or unassociated gamma-ray sources listed in the *Fermi* catalogs. Confirming RWBLs is a challenging task since they could be confused with white dwarfs (WDs) or weak emission line quasars (WELQs) when there are not sufficient data to precisely draw their broadband spectral energy distribution, and their classification is mainly based on a featureless optical spectra. Motivated by the recent discovery that *Fermi* BL Lacs appear to have very peculiar mid-IR emission, we show that it is possible to distinguish between WDs, WELQs, and BL Lacs using the [3.4]–[4.6]–[12] μm color–color plot built using the *WISE* magnitudes when the optical spectrum is available. On the basis of this analysis, we identify WISE J064459.38+603131 and WISE J141046.00+740511.2 as the first two genuine RWBLs, both potentially associated with *Fermi* sources. Finally, to strengthen our identification of these objects as true RWBLs, we present multifrequency observations for these two candidates to show that their spectral behavior is indeed consistent with that of the BL Lac population.

Key words: BL Lacertae objects: general – galaxies: active – quasars: emission lines – quasars: general – radiation mechanisms: non-thermal

1. INTRODUCTION

BL Lac objects constitute the most elusive class of radio-loud active galactic nuclei (AGNs; Urry & Padovani 1995). Hosted in elliptical galaxies (see, e.g., Falomo et al. 2014), their emission extends from radio frequencies up to the highest teraelectronvolt energies and is characterized by rapid and large-amplitude flux variability, flat radio spectra, even below ~1 GHz (see, e.g., Massaro et al. 2013a, 2013c), peculiar infrared (IR) colors (Massaro et al. 2011b; D'Abrusco et al. 2012), and significant and variable optical polarization (i.e., $P \sim 10\%$) (see, e.g., Andruchow et al. 2005; Smith et al. 2007, and references therein).

BL Lacs show featureless optical spectra, sometimes having weak emission lines of rest-frame equivalent width (EW_r) lower than 5 Å or absorption lines due to their host galaxies, both superimposed on a blue continuum (see, e.g., Laurent-Muehleisen et al. 1999). BL Lac objects are one of the two subclasses of the radio-loud AGNs known as blazars (see, e.g., Massaro et al. 2009, for a recent review). The other subclass is constituted by the flat-spectrum radio quasars (FSRQs), characterized by properties similar to those of BL Lacs but having quasar-like optical spectra (i.e., with broad emission lines; see, e.g., Véron-Cetty & Véron 2000) and radio spectral indices[9] lower than 0.5 between ~300 MHz and a few gigahertz (see Massaro et al. 2014a, and references therein).

Over the entire electromagnetic spectrum, both BL Lacs and FSRQs feature typical double-bump spectral energy distributions (SEDs), with the first component peaking between the IR and the X-ray and the second one in the gamma-ray range (see, e.g., Padovani & Giommi 1995; Paggi et al. 2009; Abdo et al. 2010b). Mid-IR colors clearly help to determine the energy peak location of the low-energy component (Massaro et al. 2011b). BL Lac SEDs and their broadband features were described in terms of emission arising from particles accelerated in relativistic jets directly pointing toward the observer (Blandford & Rees 1978).

BL Lacs are traditionally discovered using radio, X-ray surveys, or their combination (see, e.g., Stickel et al. 1991; Sambruna et al. 1996; Giommi et al. 2005), since in the optical energy range the lack of spectral features combined with their flux variability makes a color–color selection extremely challenging (Jannuzi et al. 1993; Londish et al. 2002; Collinge et al. 2005; Plotkin et al. 2008). However, recent observations to search for optical polarization in BL Lacs selected using deep optical surveys like the Sloan Digital Sky Survey (see, e.g., SDSS DR12; Alam et al. 2015, and references therein) and the Two-Degree Field Quasar Redshift Survey (2QZ; Smith et al. 2005, and references therein) validated this strategy of investigating proper motion and broadband color properties to minimize contamination by featureless Galactic objects while searching for quasi-featureless spectra (Smith et al. 2007).

At the current moment, the most efficient survey for discovering new BL Lacs is the *Fermi* gamma-ray one (Abdo et al. 2010b; Ackermann et al. 2011a; Nolan et al. 2012), in particular when combining gamma-ray observations with mid-IR color analyses (Massaro et al. 2012b, 2012c) and follow-up optical spectroscopic observations (Paggi et al. 2013; Shaw et al. 2013; Massaro et al. 2015b, 2015c; Landoni et al. 2015).

[9] Spectral indices, α, are defined by flux density, $S_\nu \propto \nu^{-\alpha}$.

This occurs because BL Lacs are the largest known population emitting at megaelectronvolt to gigaelectronvolt energies, constituting more than 30% of the associated sources in the latest release of the *Fermi* catalog (the *Fermi* Large Area Telescope Third Source Catalog, 3FGL; Acero et al. 2015). Moreover, recent optical spectroscopic campaigns aiming to confirm the nature of blazar candidates of uncertain type listed in the 3FGL showed that a significant fraction of those observed to date are also BL Lacs (see, e.g., Álvarez-Crespo et al. 2016a, 2016b, 2016c).

However, nowadays, all of the known *Fermi* BL Lacs have radio counterparts, and radio surveys are therefore crucial in associating γ-ray objects with their counterparts. Thus, one of the major open issues for this rare AGN class is proving the existence of radio-weak BL Lac objects (RWBLs). We indicate them as radio-weak sources instead of using the term "radio-quiet," generally adopted for the AGN unification scenario. This designation is more useful because radio follow-up observations could reveal some radio emission. However, the current lack of counterparts in the major radio surveys available to date place them in the tail of the distribution of the IR-to-radio flux ratios for the whole BL Lac population.

At the current moment, only a handful of sources have been claimed to be RWBLs on the basis of their broadband properties as featureless optical spectra combined with X-ray emission and their lying within the positional uncertainty regions of unidentified or unassociated gamma-ray sources (UGSs; Paggi et al. 2013; Ricci et al. 2015; Landoni et al. 2016).

Their existence will have a crucial impact (1) on the estimates of their source counts and luminosity functions (Ajello et al. 2012, 2014), a task already complicated by the challenge of measuring their redshifts (Falomo et al. 2014), (2) on the gamma-ray association methods all currently based on radio surveys (see, e.g., Ackermann et al. 2015, and references therein), if it is proved that RWBLs could be associated with *Fermi* sources, as well as (3) on the unification scenario of AGNs (Urry & Padovani 1995), to name a few implications. An accurate accounting is crucial to compute correctly their contribution to the extragalactic gamma-ray background for which, together with FSRQs (Ajello et al. 2012) and radio galaxies (Inoue 2011; Massaro & Ajello 2011a; Di Mauro et al. 2014), they provide the most significant ones. Additional implications are related to jet physics. Radio emission in extragalactic radio-loud AGNs permits us to investigate the "large-scale" (i.e., from parsec to megaparsec size) evolution of relativistic jets and their interactions with the environment (see, e.g., Fabian 2012; Liuzzo et al. 2013; Nulsen & McNamara 2013, and references therein). The existence of RWBLs could be crucial in addressing different phases of jet formation in cases when relativistic jets are not able to form extended radio structures (Blandford & Königl 1979; Begelman et al. 1984), as it seems from low radio frequency (i.e., below ~1 GHz) spectral studies (see Massaro et al. 2013c; Nori et al. 2014; Giroletti et al. 2016, and references therein).

There are two major problems to solve before claiming the existence of RWBLs, even when featureless optical spectra are available. They can be confused with or misinterpreted as hot white dwarfs (WDs; see, e.g., Kepler et al. 2015) or weak emission line quasars (WELQs; Diamond-Stanic et al. 2009; Plotkin et al. 2010, and references therein) when optical spectroscopic data are available. Optical polarimetric observations could shed light on their nature. However, unfortunately, optical polarization in BL Lacs can be variable and is not always observed, so it does not represent the most definitive stamp to confirm their nature (see, e.g., Londish et al. 2004).

In the present paper, we explore the use mid-IR colors as a diagnostic tool to disentangle BL Lacs, WDs, and WELQs. This new tool could potentially open a new window to search for RWBLs. This investigation is motivated by the recent discovery that *Fermi* BL Lacs show peculiar mid-IR colors (see also Massaro & D'Abrusco 2016 and references therein), a result made possible by observations performed with the *WISE* all-sky survey (Wright et al. 2010), covering a region well isolated from that of other Galactic and extragalactic objects. The main explanation underlying this distinction is the BL Lac nonthermal IR emission (see, e.g., D'Abrusco et al. 2012, 2013).

This paper is organized as follows. In Section 2 we present all the samples used to perform our mid-IR color–color analysis. In Section 3 we compare the mid-IR colors of BL Lacs with those of WELQs and WDs, and in Section 4 we search for RWBLs. Section 5 is dedicated to the analysis of the IR variability for the best candidates selected on the basis of the mid-IR colors and the optical spectra. Then in Section 6 we also investigate the *SWIFT* observations available for these candidates, and in Section 7 we discuss the SEDs. A summary and conclusions are given in Section 8.

Unless stated otherwise, for our numerical results, we use cgs units. *WISE* magnitudes used here are in the Vega system and are not corrected for the Galactic extinction. As shown in our previous analyses, such corrections mostly affect the magnitude at 3.4 μm for sources lying at low Galactic latitudes, and it ranges only between 2% and 5% (see, e.g., D'Abrusco et al. 2014) and is thus negligible. In addition, this allows us to compare plots in the present analysis with those of previous investigations (Massaro et al. 2013b).

2. SAMPLE SELECTION

To perform our analysis, we built three main samples. The first two are composed of WDs and WELQs; both are used in comparison with the third one of *Fermi* blazars. We searched for mid-IR counterparts of all samples in the latest release of the *WISE* catalog.[10] All of our final samples of WDs, WELQs, and gamma-ray blazars only include sources having a *WISE* counterpart within 3.″3 that is detected at 3.4, 4.6, and 12 μm, allowing us to build at least one of the mid-IR color–color plots used in our previous blazar analyses (D'Abrusco et al. 2014; Massaro & D'Abrusco 2016). The 3.″3 association radius chosen here is the same as was adopted in our previous investigations (D'Abrusco et al. 2013), and it was computed on the basis of a Monte Carlo procedure corresponding to a probability of having spurious associations of ~1% (see also D'Abrusco et al. 2014, for additional details).

2.1. BL Lac Objects and FSRQs

The first sample used in our analysis lists all the blazars, both BL Lacs and FSRQs, included in the *Roma-BZCAT*[11] (Massaro et al. 2015a) and having a counterpart in the latest release of the

[10] http://wise2.ipac.caltech.edu/docs/release/allwise/
[11] http://www.asdc.asi.it/bzcat/

Fermi catalog (Acero et al. 2015). This sample has been recently used to perform an analysis on the IR–gamma-ray connection (Massaro & D'Abrusco 2016). According to the nomenclature proposed in the *Roma-BZCAT,* we will refer to BL Lac objects as BZBs and to the FSRQs as BZQs. We choose this sample because it has the largest fraction of BZBs with a mid-IR counterpart in *WISE,* corresponding to 603 out of 610 (i.e., ∼99%) within our association radius; this fraction is similar to that occurring for the BZQs, with 419 out of 426 (i.e., ∼98%).

2.2. White Dwarfs

Hot WDs could be misclassified as BZBs because they can show almost featureless optical spectra and X-ray radiation (see, e.g., Heuse 1985; Bilková et al. 2010). Thus in the present analysis we want to show that the mid-IR colors of the *WISE* counterparts of WDs are different from that of BZBs. We expect that for WDs mid-IR emission arises from the presence of a companion brown dwarf or the presence of a dusty disk[12], both expected to have thermal IR colors (Debes et al. 2011), while those of BZBs are dominated by the nonthermal synchrotron radiation of particles accelerated in their jets.

To achieve this goal, we considered the Sloan Digital Sky Survey DR7 White Dwarf Catalog (SDSSDR7WD) (Kleinman et al. 2013). This new catalog of spectroscopically confirmed WDs from the Sloan Digital Sky Survey (SDSS) Data Release 7 (DR7) lists more than 19,000 stars. Cross-matching the SDSSDR7WD catalog with the latest release of the *WISE* catalog, we found 4,125 have a unique mid-IR potential counterpart within 3.″3. However, only for 255 out of 4,125 sources were their mid-IR counterparts detected by *WISE* in all three of its short-wavelength bands, so we only do a comparison with this subset.

We assume that mid-IR correspondences found for the SDSSDR7WD are the real counterparts of the WDs. However, in the worst-case scenario, if none of the WDs listed in the SDSSDR7WD has mid-IR emission, this will automatically confirm that their mid-IR spectral behavior is different from that of *Fermi* BZBs known to date. We also computed the chance probability of having spurious associations within 3.″3 when cross-matching the AllWISE source catalog with the SDSSDR7WD; the result is less than 4% (see, e.g., D'Abrusco et al. 2013, for more details on the method adopted for the pchance calculation).

To verify the reliability of our choice for the WD sample, we also used the latest release of the McCook & Sion White Dwarf Catalog[13] available to date (see McCook & Sion 1999 for details). This catalog has also been used to search for dusty disks around WDs (Hoard et al. 2013) using *WISE* observations. However, in this sample, the number of sources detected at 3.4, 4.6, and 12 μm for which it is possible to build the mid-IR colors is only 91. The chance probability of spurious associations between the McCook and Sion WD catalog and the ALLWISE survey is lower than 1%.

2.3. Weak Emission Line Quasars

In the last two decades, an intriguing and also elusive subclass of radio-quiet quasars was discovered: the WELQs, featuring exceptionally weak or completely missing broad emission lines in the ultraviolet (UV) rest-frame energy range (see, e.g., Collinge et al. 2005; Shemmer et al. 2006; Diamond-Stanic et al. 2009).

The original criterion to define WELQs with respect normal quasars is based on the EW$_r$ distribution of the Lyα λ1216 +N V λ1240 blend for a sample of quasars in the SDSS; at redshift $z > 3$, it is lower than 15 Å, as occurs for the $>3\sigma$ weak tail of the EW$_r$[Lyα + N V] distribution. Using this definition, a first sample of ∼70 WELQs was defined (Diamond-Stanic et al. 2009). Since at low z it is not always possible to apply the original criterion on the EW$_r$[Lyα + N V] because these emission lines lie outside the optical energy range covered by the SDSS spectrograph, an equivalent criterion was defined selecting WELQs on the basis of the EW of Mg II λ2800, C III] λ1909, or C IV λ1549 (see, e.g., Meusinger & Balafkan 2014).

When WELQs were discovered, the possibility of being classified as BZBs was explored and discarded (see, e.g., Plotkin et al. 2015, for a recent review). However, a comparison of their mid-IR properties with those of confirmed BZBs has not yet been completely performed. Here we selected a sample of WELQs to show that their mid-IR colors are generally similar to those of normal quasars but not to BZBs. Additional analyses based on the SEDs or broadband spectral indices (i.e., radio-to-optical $\alpha_{\rm ro}$ and optical-to-X-ray $\alpha_{\rm ox}$) were also used to distinguish between WELQs and BL Lacs (Plotkin et al. 2010; Lane et al. 2011; Wu et al. 2012) when multifrequency observations are available. Thus in the following sections we also investigate the broadband SEDs of RWBL candidates selected on the basis of the combination of the mid-IR colors and the optical spectra.

We considered two catalogs of WELQs, spectroscopically selected from the SDSS. The first catalog lists 73 WELQs in the redshift range between 3.03 and 5.09 (Diamond-Stanic et al. 2009, hereinafter the DS9 subsample), while the second lists 46 sources with $0.614 < z < 3.351$ (Meusinger & Balafkan 2014, hereinafter the M14 subsample). We excluded six sources out of these 119 WELQs, namely SDSS J074451.36+292006.0 and SDSS J092145.37+233548.1 from the M14 subsample and SDSS J141318.86+450522.9 from the DS9 subsample because they are all listed in the *Roma-BZCAT*; and SDSS J104831.29+211552.2, SDSS J115326.70 +361726.3, and SDSS J144204.03+132916.0, again from the M14 subsample since they show a flat radio spectrum that is widely interpreted as a jet signature, suggesting that their quasi-featureless optical continuum marks nonthermal synchrotron emission.

Only 90 out of the remaining 113 sources arising from the combination of the DS9 and the M14 subsamples have a counterpart in the ALLWISE catalog. These 90 sources thus constitute our WELQ reference sample to carry out the comparison with BZB mid-IR colors. We estimated the chance probability of spurious associations between the SDSSDR7WD catalog and the *WISE* survey as being lower than a few percent.

3. BZBs, WDs, AND WELQs AT MID-IR WAVELENGTHS

In Figure 1 we show the mid-IR colors built with the 3.4, 4.6, and 12 μm magnitudes of the BZBs and BZQs in our *Fermi* blazar sample in comparison with generic infrared sources selected at high Galactic latitudes ($|b| > 50°$), to highlight their peculiar spectral behavior. Since we know that

[12] http://www.stsci.edu/~debes/wired.html
[13] http://www.astronomy.villanova.edu/WDCatalog/index.html

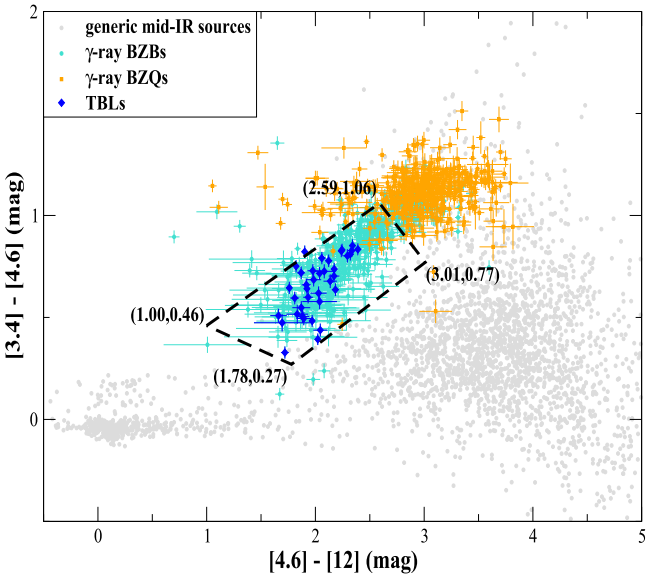

Figure 1. Mid-IR color–color plot built with the *WISE* magnitudes at 3.4, 4.6, and 12 μm. BZBs and BZQs are displayed as cyan circles and orange squares, respectively, thus corresponding to the "*WISE* gamma-ray strip" (Massaro et al. 2011b). Generic mid-IR sources (gray circles) of about 3,000 sources selected at high Galactic latitudes are also shown. The separation between the mid-IR colors of the *Fermi* blazars and that of other sources randomly chosen appears evident. The presence of BZBs in the region of the "*WISE* gamma-ray strip" occupied by the BZQs is only limited to a handful of sources (see, e.g., D'Abrusco et al. 2013, 2014, for more details). The dashed polygon marks the region used to select potential RWBLs.

BZQs generally lie in the region occupied by "normal" quasars, at the top end of the so-called "*WISE* gamma-ray strip" (Massaro et al. 2011b), to highlight the mid-IR color region where BZBs reside, we will only consider RWBL candidates from those *WISE* sources lying in the dashed polygon shown in Figure 1, where the contamination of the BZB region by BZQs is lower than 5%, lacking a radio counterpart. It is worth noting that the selected region also includes teraelectronvolt BL Lacs.

Figure 2 shows the comparison between *WISE* sources associated with WDs and our blazar sample. It is evident that only four out of the 255 sources in the SDSSDR7WD catalog have mid-IR colors consistent with the main BZB region of the "*WISE* gamma-ray strip," while the remaining ∼99% of the WDs lie well separated from this region. Three out of four sources are extragalactic, while WISE J122859.87+104032.8 has a clear WD optical spectrum, making it the only WD contaminant of the BZB region in the mid-IR color–color diagram. Moreover, WISE J122859.87+104032.8 has a negative value of $u-r$, a situation that never occurs for the known BZBs (Massaro et al. 2012a, 2014b). WISE J172633.50 +530300.3 also shows a featureless optical spectrum with a peculiar continuum shape; this could be due to the presence of a nearby source clearly visible in the SDSS image but not in the *WISE* one. This implies a relatively small contamination of the mid-IR color selection.

Both WISE J001736.91+145101.9 and WISE J121348.83 +642520.0 are BL Lacs with a radio counterpart, in addition to WISE J121348.83+642520.0 listed in the latest release of the *Roma-BZCAT* catalog.

To complete our comparison between WDs and BZBs, we also show the mid-IR color–color plot with the 91 sources selected from the McCook & Sion WD catalog in Figure 2. There are also in this case only two objects that could be confused as BZBs on the basis of their mid-IR colors, namely WISE J085506.13+063904.1 and WISE J115642.21 +130603.9, both lying in the footprint of the SDSS. Thus in both cases we checked the optical images using the SDSS Navigate tool.[14] We found that about 6.″6 from the location of WISE J085506.13+063904.1 there is a clear WD, namely SDSS J085506.62+063904.7, for which an optical spectrum is available and which is most likely the star listed in the McCook & Sion WD catalog and lacking a *WISE* counterpart. This misassociation is due to the positional uncertainty of the sources in the McCook & Sion WD catalog. Thus we conclude that WISE J085506.13+063904.1 is a simple contaminant unrelated to the WD selection. Then for the latter, WISE J115642.21+130603.9, the lack of its optical spectrum combined with the uncertainties of the SDSS photometric observations does not allow us to verify its nature. However, this object is classified as a *galaxy* and is thus unlikely to be a WD that can contaminate our RWBL selection.

The comparison between mid-IR colors of BZBs and WDs proves the usefulness of the mid-IR color diagram to distinguish the two classes while searching for RWBLs, once optical spectra are available.

Figure 3 shows the mid-IR comparison between the WELQs and the BZBs. Here too the neat separation between these two classes is clear. It is also worth noting that sources in the DS9 subsample appear to lie in a different region of the color parameter space with respect to the M14 subsample. The reason underlying this effect is their different redshift distributions. We note that there is also a marginal difference between the mid-IR colors of the WELQs in the M14 sample and that of the BZQs, but it is less useful to search for RWBLs hidden among this sample.

In this case, we highlight the fact that two WELQs lie below the threshold marking the BZB region of the color–color plot, and three additional objects are close to it. These two sources are WISE J001514.87–103043.4 and WISE J150427.69 +543902.2; both show the Mg IIλ2798 emission line with a rest-frame equivalent width EW$_r$ consistent with the 5 Å threshold, usually adopted to classify BL Lacs, within 3σ, and thus are "borderline cases." The remaining three sources, belonging to the M14 subsample (see Figure 4, where they are shown in magenta), all have a radio counterpart at 1.4 GHz in the Faint Images of the Radio Sky at Twenty centimeter (FIRST; Helfand et al. 2015) catalog, but the lack of additional radio data did not allow us to verify the flatness of their radio spectra, although they are definitely not RWBLs. The location of all five sources with respect to that of the BZBs in the mid-IR color–color plot is shown in Figure 4.

Finally, we conclude that both WDs and WELQs have distinct mid-IR colors with respect to the BL Lac population, and the [3.4]–[4.6]–[12] μm color–color diagram can be used as a diagnostic tool to confirm the source has featureless optical spectra. Sources that appear to be contaminants of the mid-IR selection procedure are ruled out when *WISE* data are combined with optical spectroscopic observations.

4. RADIO-WEAK BL LACS

In the literature, five sources are tentatively classified as RWBLs:

[14] http://skyserver.sdss.org/dr12/en/tools/chart/navi.aspx

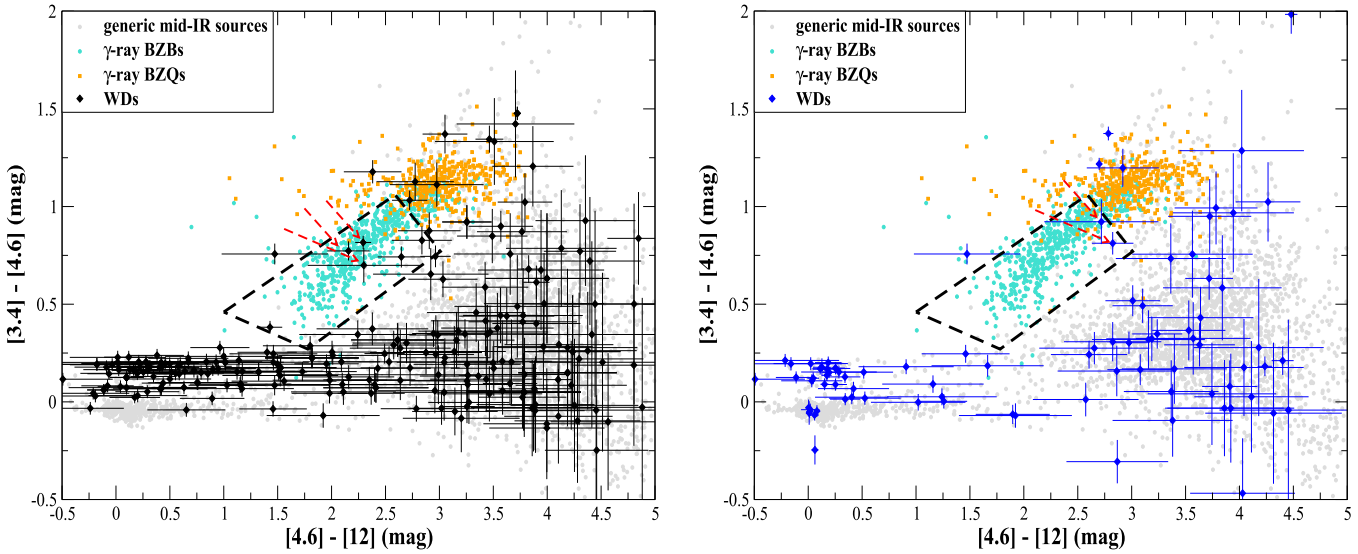

Figure 2. Comparison between the mid-IR colors of the BZBs and BZQs as shown in Figure 1 and those of the WDs (black and blue circles) from the SDSSDR7WD (left panel) and the McCook & Sion WD (right panel) catalogs, respectively. In both comparisons, the mid-IR colors of blazars appear well distinct from those of WDs, with only the few exceptions discussed in Section 3 and marked by the red arrows. Generic mid-IR sources are also shown in the background in both panels. Uncertainties on the mid-IR colors of BZBs and BZQs are not reported here as in Figure 1 for the sake of simplicity since they are shown here for comparison only.

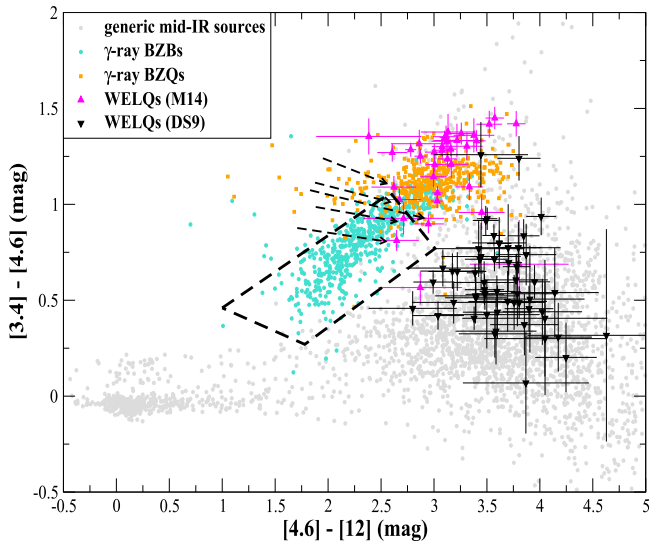

Figure 3. Comparison between the mid-IR colors of the BZBs and the BZQs as shown in Figure 1 and those of the WELQs. The WELQs belonging to the M14 subsample are shown in magenta triangles (pointing up) while those of the DS9 subsample in black triangles (pointing down). In both comparisons, the mid-IR colors of blazars appear well distinct from those of WELQs, with only the few exceptions discussed in Section 3 and marked here by the black arrows. Generic mid-IR sources are also shown in the background in both panels. Uncertainties on the mid-IR colors of BZBs and BZQs are not reported here as in Figure 1 for the sake of simplicity since they are shown here for comparison only.

1. 2QZ J215454.3–305654 (Londish et al. 2002), for which several multifrequency follow-up observations have been performed to date, was the first. However, its nature is still uncertain since it could be an RWBL or a "lineless" quasar (Londish et al. 2004).
2. Paggi et al. (2014) carried out optical spectroscopic observations of blazar candidates and potential UGS counterparts and discovered WISE J064459.38+603131. This mid-IR source lies within the positional uncertainty region of 2FGL J0644.6+6034.7 (3FGL J0644.6+6035). This object shows a single optical emission line of EW consistent with the 5 Å threshold, arbitrarily set in the literature for the BL Lac class definition, similar to the two cases discussed at the end of Section 3.
3. In 2015, WISE J173052.85–035247.2 was discovered during the optical spectroscopic follow-up observations of UGSs (Ricci et al. 2015). This source could be the potential counterpart of 2FGL J1730.6–0353 (also known as 3FGL J1730.6–0357).
4. More recently, Landoni et al. (2016) claimed that SDSS J004054.65–0915268 could also be a tentative RWBL.
5. Finally, Marchesini et al. (2016) discovered the last known candidate of RWBL, WISE J141046.00+740511.2. This source was also found while carrying out spectroscopic observations of UGSs listed in the First *Fermi*-LAT Catalog of Sources above 10 GeV (1FHL; Ackermann et al. 2013), selected on the basis of the *SWIFT* X-ray observations (Landi et al. 2015). It has been indicated as a potential counterpart of 1FHL J1410.4+7408 (also known as 3FGL J1410.9+7406).

In Figure 4 we show the positions of the five RWBLs overlaid on the "*WISE* gamma-ray strip" subregion of BZBs. SDSS J004054.65–0915268 (also known as WISE J004054.63–091526.8) has an upper limit at 12 μm, and being a high-z source, it seems to be more consistent with the location of the DS9 subsample of WELQs rather than the BZB population. A similar situation occurs for 2QZ J215454.3–305654 (also known as J215454.32–305653.2), for which only follow-up observations at 12 μm could potentially reveal if the source is consistent with the mid-IR colors of the BZBs. WISE J064459.38+603131.7, being selected on the basis of its mid-IR colors, is definitely consistent with the BZB population on the 3.4 μm–4.6 μm–12 μm diagram, while WISE J173052.85–035247.2 appears to have colors that are more similar to the WELQs listed in the M14 subsample.

The remaining case of WISE J141046.00+740511.2 is the most intriguing one. This object is potentially associated with a 1FHL object, and its potential *WISE* counterpart lies in the region of the "*WISE* gamma-ray strip" where all known

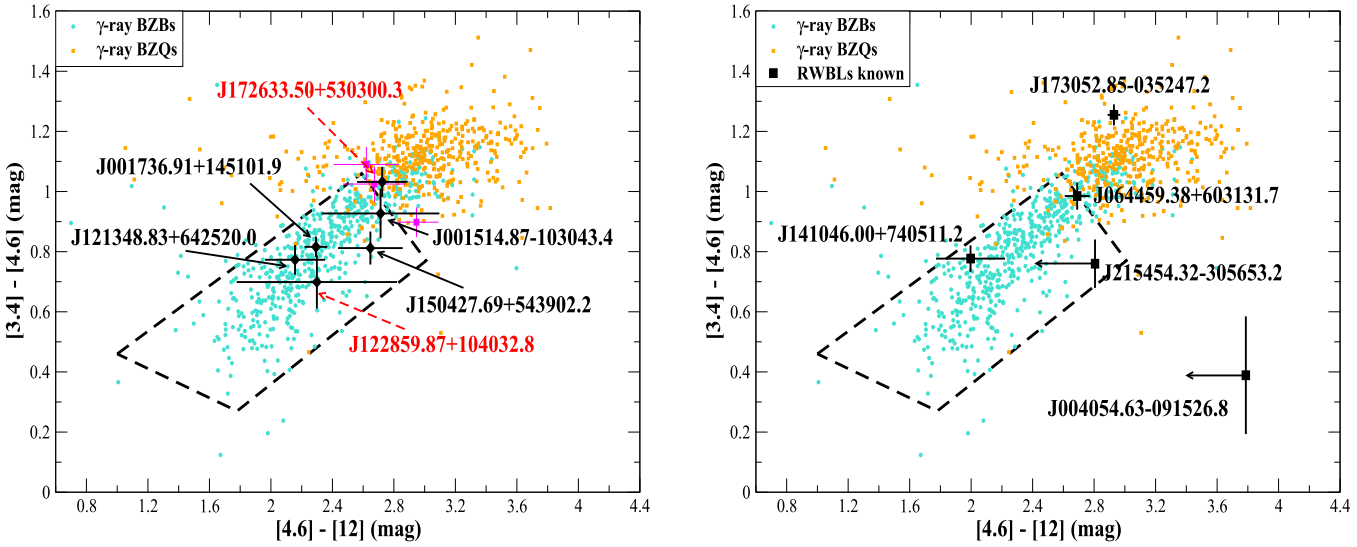

Figure 4. Left panel: the mid-IR color–color plot where the positions of the blazars recognized in the WD and the WELQ samples are highlighted with respect to the *Fermi* blazars. WISE J122859.87+104032.8 and WISE J172633.50+530300.3 are marked with a red arrow since additional optical information allows us to discard them as potential RWBLs. The former has the unusual negative value of the $u - r$ never seen for BL Lacs, while the mid-IR colors of the latter are contaminated by the presence of a nearby source visible in the optical image (see Section 3 for more details). Right panel: the positions of the candidate RWBLs in the mid-IR color–color plot are shown in comparison to that of *Fermi* blazars belonging to the "*WISE* gamma-ray strip" and those of generic mid-IR sources (same color code as in previous figures). Source details for the objects indicated in both panels are given in Section 3. Uncertainties on the mid-IR colors of BZBs and BZQs are not reported here as in Figure 1 for the sake of simplicity since they are shown here for comparison only.

teraelectronvolt BL Lacs are located (Massaro et al. 2013d; Arsioli et al. 2015). The lack of any radio counterpart in the NRAO VLA Sky Survey (NVSS; Condon et al. 1998), which covers the field of WISE J141046.00+740511.2, makes this source the most promising candidate to be the first, genuine RWBL. Nevertheless, it is worth emphasizing that the distance between this mid-IR source and the gamma-ray position of 3FGL J1410.9+7406 is ∼90″, well below the average of the associated *Fermi* blazars listed in the *Roma-BZCAT*, corresponding to ∼130″. At the angular separation of ∼90″, the association probabilities of the counterparts listed in the latest releases of the *Fermi* catalogs are typically greater than 99.5% (Ackermann et al. 2015).

Applying this mid-IR color-based analysis, in combination with optical spectra, we conclude that WISE J064459.38 +603131 and WISE J141046.00+740511.2, lying within the positional uncertainty regions of two distinct UGSs listed in the 3FGL, are the first two RWBLs detected so far. Both of them can also be associated with 1FHL sources, thus strengthening our interpretation, since the high-energy sky above 10 GeV is mostly dominated by BZBs. In the following, we will also show that additional multifrequency observations can strengthen our results.

5. MID-IR VARIABILITY

BL Lac objects are known to be among the most variable extragalactic sources at all frequencies, showing variations either in spectral shape or in flux or luminosities. This peculiar behavior could in principle undermine the mid-IR color selection proposed here and in our previous works. However, this situation does not seem to occur.

BL Lacs appear to be variable in the mid-IR band (see, e.g., D'Abrusco et al. 2012), although their color variations still reside within the boundaries of the "*WISE* gamma-ray strip" (see S. Buson et al. 2016, in preparation, for more details). Here

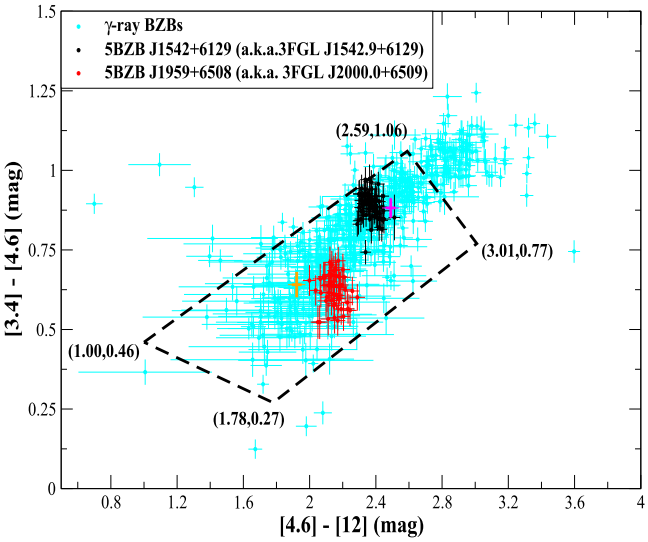

Figure 5. Mid-IR color–color plot built with the *WISE* magnitudes at 3.4, 4.6, and 12 μm. BZBs are displayed as cyan circles and correspond to the "*WISE* gamma-ray strip" (Massaro et al. 2011b). We show two clusters of points relative to the *WISE* single-epoch observations of the BZBs: 5BZBJ1542 +6129 (black circles) and 5BZBJ1959+6508 (red circles). It appears evident that even the mid-IR color variation states of these two BL Lac objects are always consistent with the boundaries of the "*WISE* gamma-ray strip." The two crosses point to the location of 5BZBJ1542+6129 (magenta) and 5BZBJ1959 +6508 (orange) on the mid-IR color diagram when integrated values for the entire *WISE* all-sky survey are used.

we show an example of two BZBs: 5BZBJ1542+6129 and 5BZBJ1959+6508, the latter also detected at teraelectronvolt energies (Aharonian et al. 2003), for which more than 50 *WISE* observations are available, when both sources are detected at least in the first three mid-IR filters at 3.4, 4.6, and 12 μm. In Figure 5 it is clear how both BZBs during their single-epoch *WISE* observations move in the mid-IR color–

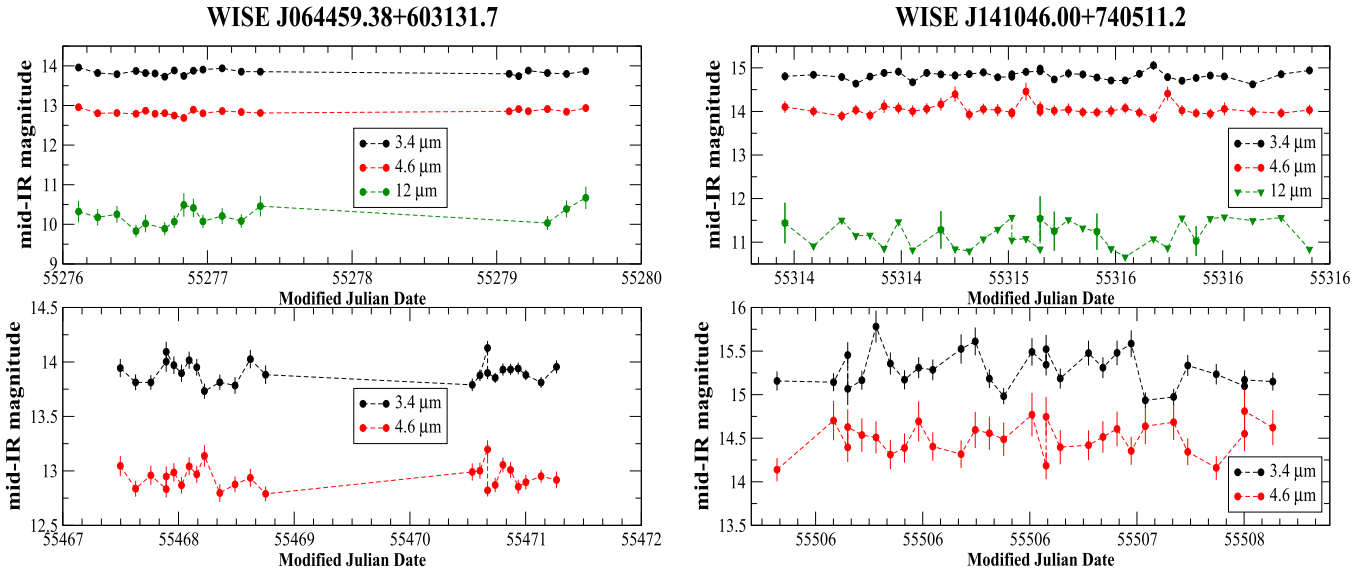

Figure 6. Light curves of WISE J064459.38+603131 (left panel) and WISE J141046.00+740511.2 (right panel), candidate RWBLs, tentatively associated with 3FGL and 1FHL *Fermi* sources. These are *WISE* single-epoch observations for two different time periods. Mid-IR flux density is expressed using the *WISE* magnitude (not corrected for absorption) as a function of time in Modified Julian Date. Each epoch (top and bottom panels) corresponds to approximately two days. Infrared variability is clearly notable for both sources. Triangles are used to mark *WISE* observations that correspond to upper limits at a given wavelength.

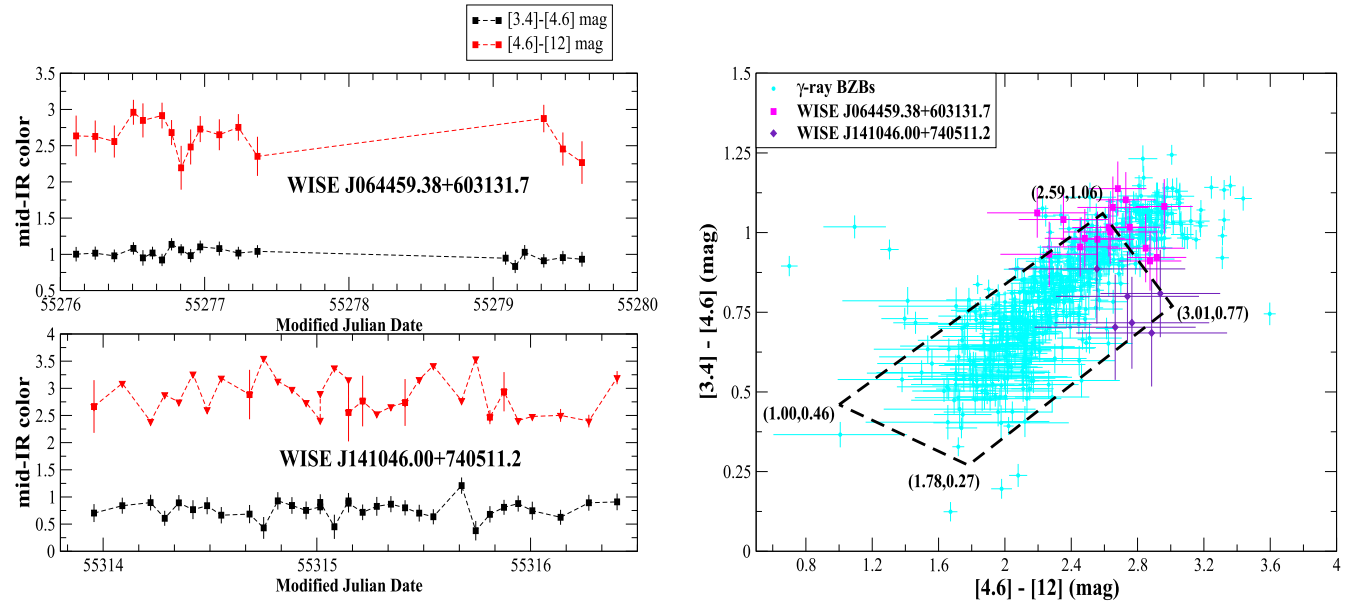

Figure 7. Left panel: mid-IR colors reported as a function of time in Modified Julian Date for both RWBLs selected in our analysis: WISE J064459.38+603131 (top) and WISE J141046.00+740511.2 (bottom). For WISE J064459.38+603131, we only considered *WISE* observations when the source is detected in all three filters, while for WISE J141046.00+740511.2 we computed the [4.6]–[12] μm color light curve also using the upper limits (red triangles pointing down). Right panel: same as Figure 5 but for the two RWBLs selected: WISE J064459.38+603131 (purple squares) and WISE J141046.00+740511.2 (magenta diamonds). The variations found in the single-epoch *WISE* observations when both sources are detected in the first three mid-IR filters are clearly consistent with the boundaries of the portion of the "*WISE* gamma-ray strip" for WISE J141046.00+740511.2 and partially in agreement for WISE J064459.38+603131.

color plot in the same region occupied by the BL Lac objects. In addition, their colors are also consistent with the boundaries chosen for our RWBL selection procedure.

According to the *WISE* catalog, one of our best RWBL candidates, WISE J141046.00+740511.2, is flagged as variable in the mid-IR. This is in agreement with the fact that such emission is unlikely due to dust emission, as occurs in normal quasars or in WDs (Debes et al. 2011). Figure 6 shows the *WISE* magnitude at 3.4, 4.6, and 12 μm as a function of time for two different epochs; mid-IR variability, not only between the two observing periods but also in each single set of observations, is found. We also present the light curve for the second RWBL candidate WISE J064459.38+603131, which clearly shows infrared variability being detected more times at 12 μm during the *WISE* single-epoch observations with respect to WISE J141046.00+740511.2.

In Figure 7 we also show their mid-IR color variability as a function of time. In the same figure, we also present the single-epoch observations when both sources are detected in the first three *WISE* filters overlaid on the "*WISE* gamma-ray strip." As for the other two BZBs mentioned above, these variations are clearly consistent with the region chosen to select

RWBLs for WISE J141046.00+740511.2, while for WISE J064459.38+603131 there is partial agreement. It is worth mentioning that the location of integrated mid-IR colors for both WISE J064459.38+603131 and WISE J141046.00 +740511.2 could appear different from that where they exhibit variability in the mid-IR color diagram. The underlying reason is that there are many *WISE* single-epoch observations when sources (see Figure 6) are not detected that contribute to the color change for the integrated values. It is also worth noting that for the two RWBL candidates the uncertainties on the *WISE* magnitudes are greater than for the two bright BZBs selected above as examples.

On the basis of this investigation of mid-IR variability and spectral behavior, we conclude that the evidence supports the interpretation of these sources as RWBLs.

6. *SWIFT* OBSERVATIONS

Several analyses were carried out to study the nature of WELQs in the X-ray (see, e.g., Shemmer et al. 2009; Wu et al. 2012). These observations were also used to build their broadband spectral indices or their SEDs (see, e.g., Plotkin et al. 2010) to verify their potential similarities with BL Lac objects. Since the two sources identified here as RWBLs were discovered during a campaign aimed at searching for UGS counterparts and all of the *Fermi* UGSs are in a *SWIFT* observational program (Stroh & Falcone 2013),[15] we reduced the *SWIFT* data available to date to build the RWBL SEDs.

WISE J064459.38+603131 was observed by *SWIFT* both with the X-Ray Telescope (XRT), for ∼3 ks, and with the Ultraviolet/Optical Telescope (UVOT) instruments on board, but for the latter the only ultraviolet filter used was M2. On the other hand, for WISE J141046.00+740511.2, there are optical data in the *U* band and all the UV filters available, together with about 11 ks of X-ray data.

Here we adopted the standard XRT and UVOT data-reduction procedure, extensively used in our previous analyses (see, e.g., Massaro et al. 2008b; Maselli et al. 2013, 2016, and references therein), and only the very basic details are described below. XRT data were processed with the XRTDAS software package (v.3.0.0) developed at the ASI Science Q9 Data Center (ASDC) and distributed within the HEASOFT package (v.6.18) by the NASA High Energy Astrophysics Archive Research Center (HEASARC). All of the XRT observations were carried out in the photon counting (PC) readout mode. Event files were calibrated and cleaned, applying standard filtering criteria with the *XRTPIPELINE* task and using the latest calibration files available in the *Swift* CALDB. Events in the energy range of 0.3–10 keV with grades 0–12 were selected in the analysis according to the standard guidelines. Exposure maps were also created using *XRTPIPELINE*. The *SWIFT* observations available for both sources have variable exposures, so we merged cleaned event files obtained with the above procedure using the *XSELECT* task and considering only *SWIFT* observations with the telescope aim point falling in a circular region of 12 arcmin radius centered in the median of the individual aim points, to get a uniform exposure. The corresponding merged exposure maps were then generated by summing the exposure maps of the individual observations with the *XIMAGE* package. Source detection in the XRT images was performed using the detection algorithm *DETECT*.

We collected 13 counts for WISE J064459.38+603131 in the merged XRT event file, and there are 36 counts for WISE J141046.00+740511.2, making both sources well detected above the 5σ threshold. However, the poor number of counts available, corresponding to count rates of $0.004\,\mathrm{cts\,s^{-1}}$ and $0.003\,\mathrm{cts\,s^{-1}}$, respectively, did not permit us to carry out a detailed spectral analysis. Thus assuming an absorbed power-law model with a photon index of 2.2 and with the Galactic hydrogen column density (Kalberla et al. 2005), we estimated the unabsorbed X-ray flux in the 0.5–10 keV region for WISE J064459.38+603131 and for WISE J141046.00+740511.2 using WebPIMMS.[16]

Details on the UVOT reduction procedure used here are described in Massaro et al. (2008a) and Maselli et al. (2008). We performed the photometric analysis using a standard task *UVOTSOURCE* available in the HEASOFT package (v.6.18). Counts were extracted from a 5 arcsec radius circular region in the V, B, and U filters as well as for the UV filters (UVW1, UVM2, and UVW2). The count rate was corrected for coincidence loss, and the background subtraction was performed by estimating its level in an offset annular region centered on the source position with inner radius of 7.5 arcsec and outer radius of 15 arcsec. Since the estimation of magnitude errors is complex, due to possible instrumental systematics and calibration, here we only showed a typical uncertainty of 5% for all filters.

The value of the observed AB magnitude for WISE J064459.38+603131 in the UV band at 1.36×10^{15} Hz is 19.69 mag (M2 UVOT filter), while for WISE J141046.00 +740511.2 the AB magnitudes measured in the UVOT filters are 19.23 mag (U), 19.85 mag (W1), 20.24 mag (M2), and 20.31 mag (W2).

In Figure 8 we show the XRT event file in the 0.3–10 keV energy range and one of the UVOT images for both of the RWBLs selected. We overlaid on the *SWIFT* images the positional uncertainty region, at 95% level of confidence, from the 2FGL and 3FGL catalogs for the nearby UGSs. WISE J064459.38+603131 lies within the error ellipse of the 2FGL, as occurred when it was selected (Massaro et al. 2012b), but not within that of the 3FGL, while for WISE J141046.00 +740511.2, which is associable with the 3FGL source, a potential counterpart in the 2FGL UGS was not found.

SWIFT observations, both in the UV and in the X-ray energy ranges, are used in the following to build the SEDs for both of the RWBLs selected.

7. SPECTRAL ENERGY DISTRIBUTIONS

For the two RWBLs selected, we also built the SEDs to check whether or not they are similar to those of WELQs (Lane et al. 2011). An analysis of the SEDs is equivalent to comparing broadband spectral indices that could give an additional indication of the differences between BL Lacs and WELQs (see, e.g., Wu et al. 2012).

In the case of WISE J064459.38+603131, the source has an upper limit in the NVSS catalog of $0.13\,\mathrm{mJy\,beam^{-1}}$, while WISE J141046.00+740511.2 has $1.69\,\mathrm{mJy\,beam^{-1}}$. The former is detected in all of the *WISE* bands and in the 2MASS. From the *SWIFT* observations, we also got an estimate of the

[15] http://www.swift.psu.edu/unassociated/

[16] https://heasarc.gsfc.nasa.gov/cgi-bin/Tools/w3pimms/w3pimms.pl

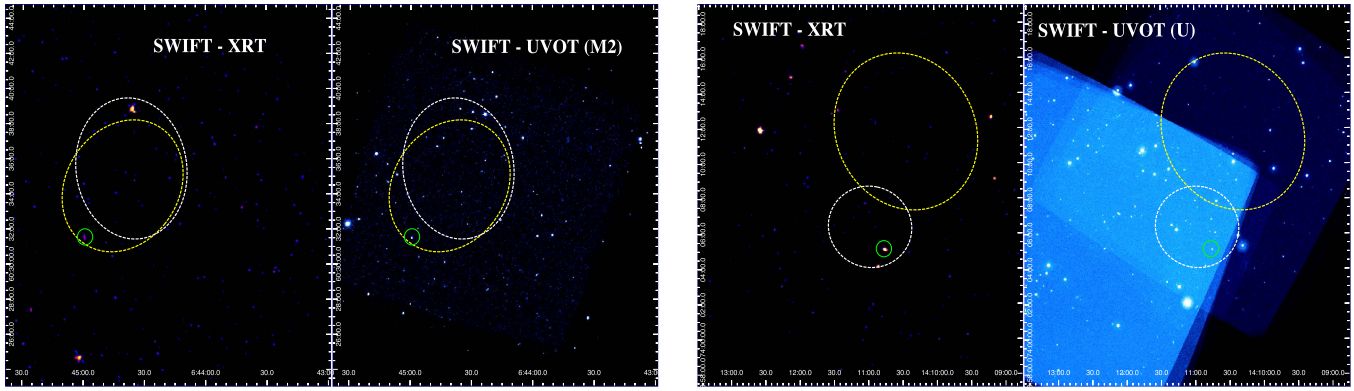

Figure 8. Left panels: the XRT (left) and the UVOT (M2 filter) images of the field where WISE J064459.38+603131 lies. The yellow dashed ellipse marks the positional uncertainty region of the closest 2FGL unassociated source, while the white one marks the error ellipse from the 3FGL catalog, both at 95% level of confidence; green circles mark the location of the X-ray counterpart. Right panel: same as top panels for WISE J141046.00+740511.2. The UVOT image in this case is in the optical energy range (i.e., the U filter) instead of the UV.

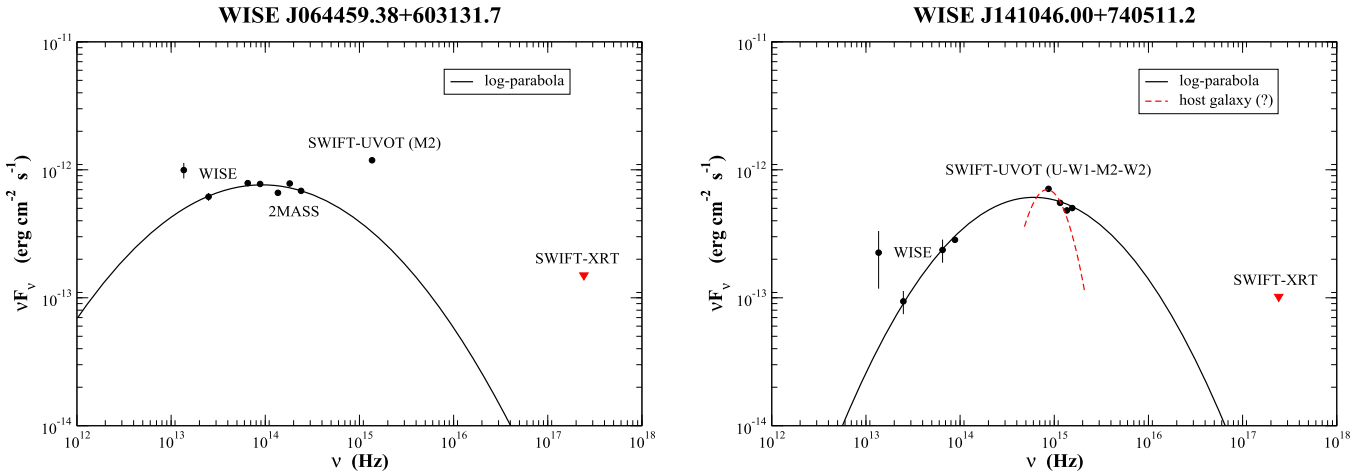

Figure 9. SEDs of both WISE J064459.38+603131 (left panel) and WISE J141046.00+740511.2 (right panel). Data points are shown as black circles, and labels indicate the telescope used to obtain them. The black line marks the broadband log-parabolic function generally adopted to describe nonthermal SEDs of BL Lacs. For WISE J141046.00+740511.2, the dashed red line points toward the host galaxy interpretation for the optical–UV data. Unabsorbed X-ray fluxes, in the 0.5–10 keV energy range, estimated from the XRT source counts are also shown as red triangles in both panels.

UV flux density in the M2 filter and the X-ray flux. The latter source still has a *WISE* counterpart detected at all mid-IR frequencies, but it does not have a 2MASS correspondence. *SWIFT* observations provided us flux density estimates in the optical (U) and in all the UV filters (W1, M2, W2) together with the X-ray one.

We corrected all of the infrared, optical, and ultraviolet flux densities for the Galactic absorption following Draine (2003) and the reddening corrections of Schlafly & Finkbeiner (2011), with the only exception for the *WISE* magnitudes at 12 and 22 μm.

In Figure 9 we show the SEDs for both WISE J064459.38 +603131 and WISE J141046.00+740511.2. For the former SED, the infrared emission appears to be compatible with a log-parabolic shape (Massaro et al. 2004, 2006), with the only exception of the UVOT flux density in the M2 filter. This could be due to the presence of the host galaxy or to variability since UV and IR observations were not taken simultaneously and both of them are integrated over different epochs. The latter source, WISE J141046.00+740511.2, also has an SED well described by a log-parabolic shape, but in this case the *SWIFT* optical and UV data seem to mark the presence of a host galaxy. In both panels of Figure 9 we also report the unabsorbed X-ray flux computed from the source counts of the XRT event file. Since this X-ray flux is an estimate, we neglect second-order corrections to convert the X-ray flux into a νF_ν SED value.

The agreement between the multifrequency data and the broadband log-parabolic SED support the interpretation of WISE J064459.38+603131 and WISE J141046.00+740511.2 as RWBLs.

8. SUMMARY AND CONCLUSIONS

1. The mid-IR colors of BL Lacs appear to be clearly different from those of WDs and WELQs. This strongly indicates that the *WISE* color–color diagram built with the mid-IR magnitudes at 3.4, 4.6, and 12 μm, together with optical spectroscopic observations, is a powerful diagnostic tool to distinguish these three source classes. We found only a few contaminants within the WD and the WELQ catalogs used in our analysis. However, for all these cases, the combination of mid-IR and optical spectroscopic data allowed us to exclude them as BL Lacs.
2. Applying this mid-IR color-based analysis, we conclude that WISE J064459.38+603131 and WISE J141046.00

+740511.2, lying within the positional uncertainty regions of two distinct UGSs, are the first two RWBLs detected so far. Both of them are also associable with 1FHL sources, thus strengthening our interpretation, since the high-energy sky above 10 GeV is mostly dominated by BZBs. Both sources appear to be variable in the mid-IR, as expected for BZBs, and they also show broadband SEDs, built thanks to the *WISE* and *SWIFT* observations, consistent with a log-parabolic shape.

3. In addition, 2QZ J215454.3–305654 could also potentially be an RWBL, but without the mid-IR detection at 12 μm, it is not possible to confirm its nature using the mid-IR color–color plot. In addition, the two contaminants WISE J001514.87–103043.4 and WISE J150427.69+543902.2, found in the WELQ sample used here, deserve a deeper investigation to clarify their nature.

We highlight that the strategy used to search for potential counterparts of UGSs via X-ray follow-up observations has been crucial in both cases in discovering WISE J064459.38+603131 and WISE J141046.00+740511.2, thus emphasizing that combining X-ray and mid-IR observations could be crucial for future searches for low-energy counterparts of gamma-ray sources. However, we also stress that this discovery has been done thanks to optical spectroscopic follow-up campaigns that finally revealed the source nature. Since both of these two sources are not only associable with 3FGL objects but also with *Fermi* sources detected above 10 GeV, their existence challenges current gamma-ray association methods mostly based on radio surveys that do not allow one to catch these potential counterparts. The existence of RWBLs will also have strong impacts on jet physics since they could allow us to study sources whose emission is dominated by relativistic jets that do not tend to form extended radio structures as their parent population of radio galaxies.

Finally, we remark that deeper radio follow-up observations than those available to date could potentially reveal their low-energy emission at gigahertz frequencies. However, the ratio between the infrared and the radio emission of so-called RWBLs, being below the flux limit of current radio surveys, is unexpectedly unusual. In Figure 10 we show the distribution of such a ratio to highlight how the two selected RWBLs lie in the tail of the BL Lac population, being below the 0.5 value.

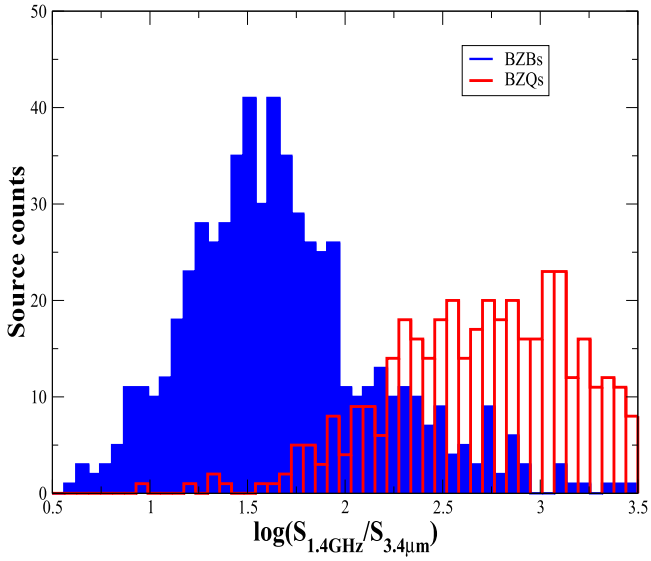

Figure 10. Distributions of the log of the ratio between the radio flux densities at 1.4 GHz and the mid-IR one at 3.4 μm for the BZBs (blue) and BZQs (red) in our sample. The two selected RWBLs lie at least on the low tail of the blue distribution drawn for the BZBs, thus making them extreme sources even if follow-up observations will reveal their radio emission.

We thank the anonymous referee for useful comments that led to improvements in the paper. F.M. thanks D. Stern for helpful suggestions. F.M. gratefully acknowledges the financial support of the Programma Giovani "R.L. Montalcini"—Rientro dei Cervelli (2012) awarded by the Italian Ministry of Education, Universities and Research (MIUR). H.A.S. acknowledges partial support from NASA Grants NNX15AE56G and NNX14AJ61G. This research has made use of data obtained from the high-energy Astrophysics Science Archive Research Center (HEASARC) provided by NASA's Goddard Space Flight Center. The NASA/IPAC Extragalactic Database (NED) is operated by the Jet Propulsion Laboratory, California Institute of Technology, under contract with the National Aeronautics and Space Administration. Part of this work is based on the NVSS (NRAO VLA Sky Survey). The National Radio Astronomy Observatory is operated by Associated Universities, Inc., under contract with the National Science Foundation and on the VLA Low-frequency Sky Survey (VLSS). This publication makes use of data products from the *Wide-field Infrared Survey Explorer*, which is a joint project of the University of California, Los Angeles, and the Jet Propulsion Laboratory/California Institute of Technology, funded by the National Aeronautics and Space Administration. TOPCAT[17] (Taylor 2005) was used for the preparation and manipulation of the tabular data and the images.

REFERENCES

Abdo, A. A., Ackermann, M., Ajello, M., et al. 2010a, ApJ, 715, 429
Abdo, A. A., Ackermann, M., Ajello, M., et al. 2010b, ApJS, 188, 405
Acero, F., Ackermann, M., Ajello, M., et al. 2015, ApJS, 218, 23
Ackermann, M., Ajello, M., Allafort, A., et al. 2011a, ApJ, 743, 171
Ackermann, M., Ajello, M., Allafort, A., et al. 2013, ApJS, 209, 34
Ackermann, M., Ajello, M., Atwood, W. B., et al. 2015, ApJ, 810, 14
Aharonian, F., Akhperjanian, A., Beilicke, M., et al. 2003, A&A, 406L, 9
Ajello, M., Romani, R. W., Gasparrini, D., Shaw, M. S., Bolmer, J., et al. 2014, ApJ, 780, 73
Ajello, M., Shaw, M. S., Romani, R. W., et al. 2012, ApJ, 751, 108
Alam, S., Albareti, F. D., Allende Prieto, C., Anders, F., Anderson, S. F., et al. 2015, ApJS, 219, 12
Álvarez-Crespo, N., Masetti, N., Ricci, F., et al. 2016, AJ, 151, 32
Álvarez-Crespo, N., Massaro, F., D'Abrusco, R., et al. 2016, Ap&SS, 361, 316
Álvarez-Crespo, N., Massaro, F., Milisavljevic, D., et al. 2016, AJ, 151, 95
Andruchow, I., Romero, G. E., & Cellone, S. A. 2005, A&A, 442, 97
Arsioli, B., Fraga, B., Giommi, P., Padovani, P., & Marrese, P. M. 2015, A&A, 579A, 34
Begelman, M. C., Blandford, R. D., & Rees, M. J. 1984, RvMP, 56, 255
Bilková, J., Chu, Y.-H., Gruendl, R. A., & Maddox, L. A. 2010, AJ, 140, 1433
Blandford, R. D., & Königl, A. 1979, ApJ, 232, 34
Blandford, R. D., & Rees, M. J. 1978, in Pittsburgh Conf. on BL Lac Objects, ed. A. M. Wolfe (Pittsburgh, PA: Univ. Pittsburgh Press), 328
Collinge, M. J., Strauss, M. A., Hall, P. B., Ivezić, Ž., Munn, J. A., et al. 2005, AJ, 129, 2542
Condon, J. J., Cotton, W. D., Greisen, E. W., et al. 1998, AJ, 115, 1693
D'Abrusco, R., Massaro, F., Ajello, M., et al. 2012, ApJ, 748, 68
D'Abrusco, R., Massaro, F., Paggi, A., et al. 2013, ApJS, 206, 12
D'Abrusco, R., Massaro, F., Paggi, A., et al. 2014, ApJS, 215, 14
Debes, J. H., Hoard, D. W., Wachter, S., et al. 2011, ApJS, 197, 38
Diamond-Stanic, A. M., Fan, X., Brandt, W. N., et al. 2009, ApJ, 699, 782
Di Mauro, M., Calore, F., Donato, F., Ajello, M., & Latronico, L. 2014, ApJ, 780, 161
Draine, B. T. 2003, ARA&A, 41, 241

[17] http://www.star.bris.ac.uk/~mbt/topcat/

Fabian, A. C. 2012, ARA&A, 50, 455
Falomo, R., Pian, E., & Treves, A. 2014, A&ARv, 22, 73
Giommi, P., Piranomonte, S., Perri, M., & Padovani, P. 2005, A&A, 434, 385
Giroletti, M., Massaro, F., D'Abrusco, R., et al. 2016, A&A, 588A, 141
Helfand, D. J., White, R. L., & Becker, R. H. 2015, ApJ, 801, 26
Heuse, J. 1985, SSRv, 40, 79
Hoard, D. W., Debes, J. H., Wachter, S., et al. 2013, ApJ, 770, 21
Inoue, Y. 2011, ApJ, 733, 66
Jannuzi, B. T., Green, R. F., & French, H. 1993, ApJ, 404, 100
Kalberla, P. M. W., Burton, W. B., Hartmann, D., et al. 2005, A&A, 440, 775
Kepler, S. O., Pelisoli, I., Koester, D., et al. 2015, MNRAS, 446, 4078
Kleinman, S. J., Kepler, S. O., Koester, D., et al. 2013, ApJS, 204, 5
Landi, R., Bassani, L., Stephen, J. B., et al. 2015, A&A, 581, A57
Landoni, M., Massaro, F., Paggi, A., D'Abrusco, R., Milisavljevic, D., et al. 2015, AJ, 149, 63
Landoni, M., Zanutta, A., Bianco, A., et al. 2016, AJ, 151, 35
Lane, R. A., Shemmer, O., Diamond-Stanic, A. M., Fan, X., et al. 2011, ApJ, 743, 163
Laurent-Muehleisen, S. A., Kollgaard, R. I., Feigelson, E. D., et al. 1999, ApJ, 525, 127
Liuzzo, E., Buttiglione, S., Giovannini, G., et al. 2013, A&A, 550A, 76
Londish, D., Croom, S. M., Boyle, B. J., Shanks, T., Outram, P. J., Sadler, E. M., et al. 2002, MNRAS, 334, 941
Londish, D., Heidt, J., Boyle, B. J., Croom, S. M., & Kedziora-Chudczer, L. 2004, MNRAS, 352, 903
Marchesini, E. J., Masetti, N., Chavushyan, V., Cellone, S. A., Andruchow, I., et al. 2016, A&A, in press
Maselli, A., Giommi, P., Tramacere, A., et al. 2008, A&A, 479, 35
Maselli, A., Massaro, F., Cusumano, G., et al. 2013, ApJS, 206, 17
Maselli, A., Massaro, F., Cusumano, G., et al. 2016, MNRAS, 460, 3829
Massaro, E., Giommi, P., Leto, C., et al. 2009, A&A, 495, 691
Massaro, E., Maselli, A., Leto, C., et al. 2015a, Ap&SS, 357, 75
Massaro, E., Nesci, R., & Piranomonte, S. 2012a, MNRAS, 422, 2322
Massaro, E., Perri, M., Giommi, P., & Nesci, R. 2004, A&A, 413, 489
Massaro, E., Tramacere, A., Perri, M., Giommi, P., & Tosti, G. 2006, A&A, 448, 861
Massaro, F., & Ajello, M. 2011a, ApJ, 729L, 12
Massaro, F., & D'Abrusco, R. 2016, ApJ, 827, 67
Massaro, F., D'Abrusco, R., Ajello, M., et al. 2011b, ApJ, 740L, 48
Massaro, F., D'Abrusco, R., Giroletti, M., et al. 2013a, ApJS, 207, 4
Massaro, F., D'Abrusco, R., Landoni, M., et al. 2015b, ApJS, 217, 2
Massaro, F., D'Abrusco, R., Paggi, A., et al. 2013b, ApJS, 206, 13
Massaro, F., D'Abrusco, R., Tosti, G., et al. 2012b, ApJ, 752, 61
Massaro, F., D'Abrusco, R., Tosti, G., et al. 2012c, ApJ, 750, 138
Massaro, F., Giommi, P., Tosti, G., et al. 2008a, A&A, 489, 1047
Massaro, F., Giroletti, M., D'Abrusco, R., et al. 2014a, ApJS, 213, 3
Massaro, F., Giroletti, M., Paggi, A., et al. 2013c, ApJS, 208, 15
Massaro, F., Landoni, M., D'Abrusco, R., et al. 2015c, A&A, 575, 124
Massaro, F., Masetti, N., D'Abrusco, R., et al. 2014b, AJ, 148, 66
Massaro, F., Paggi, A., Errando, M., et al. 2013d, ApJS, 207, 16
Massaro, F., Tramacere, A., Cavaliere, A., Perri, M., & Giommi, P. 2008b, A&A, 478, 395
McCook, G. P., & Sion, E. M. 1999, ApJS, 121, 1
Meusinger, H., & Balafkan, N. 2014, A&A, 568A, 114
Nolan, P. L., Abdo, A. A., Ackermann, M., et al. 2012, ApJS, 199, 31
Nori, M., Giroletti, M., Massaro, F., et al. 2014, ApJS, 212, 3
Nulsen, P. E. J., & McNamara, B. R. 2013, AN, 334, 386
Padovani, P., & Giommi, P. 1995, ApJ, 444, 567
Paggi, A., Massaro, F., D'Abrusco, R., et al. 2013, ApJS, 209, 9
Paggi, A., Massaro, F., Vittorini, V., et al. 2009, A&A, 504, 821
Paggi, A., Milisavljevic, D., Masetti, N., et al. 2014, AJ, 147, 112
Plotkin, R. M., Anderson, S. F., Hall, B. W. N., et al. 2010, ApJ, 721, 562
Plotkin, R. M., Anderson, S. F., Hall, P. B., et al. 2008, AJ, 135, 2453
Plotkin, R. M., Shemmer, O., Trakhtenbrot, B., et al. 2015, ApJ, 805, 123
Ricci, F., Massaro, F., Landoni, M., et al. 2015, AJ, 149, 160
Sambruna, R., Maraschi, L., & Urry, C. M. 1996, ApJ, 463, 444
Schlafly, E. F., & Finkbeiner, D. P. 2011, ApJ, 737, 103
Shaw, M. S., Romani, R. W., Cotter, G., et al. 2013, ApJ, 764, 135
Shemmer, O., Brandt, W. N., Anderson, S. F., et al. 2009, ApJ, 696, 580
Shemmer, O., Brandt, W. N., Schneider, D. P., et al. 2006, ApJ, 644, 86
Smith, P. S., Williams, G. G., Schmidt, G. D., et al. 2007, ApJ, 663, 118
Smith, R. J., Croom, S. M., Boyle, B. J., et al. 2005, MNRAS, 359, 57
Stickel, M., Padovani, P., Urry, C. M., et al. 1991, ApJ, 374, 431
Stroh, M. C., & Falcone, A. D. 2013, ApJS, 207, 28
Taylor, M. B. 2005, in ASP Conf. Ser. 347, Astronomical Data analysis Software and Systems XIV, ed. P. Shopbell, M. Britton, & R. Ebert (San Francisco, CA: ASP), 29
Urry, C. M., & Padovani, P. 1995, PASP, 107, 803
Véron-Cetty, M. P., & Véron, P. 2000, A&ARv, 10, 81
Wright, E. L., Eisenhardt, P. R. M., Mainzer, A. K., Ressler, M. E., Cutri, R. M., et al. 2010, AJ, 140, 1868
Wu, J., Brandt, W. N., Anderson, S. F., et al. 2012, ApJ, 747, 10